PAPER

Polaromics: deriving polarization parameters from a Mueller matrix for quantitative characterization of biomedical specimen

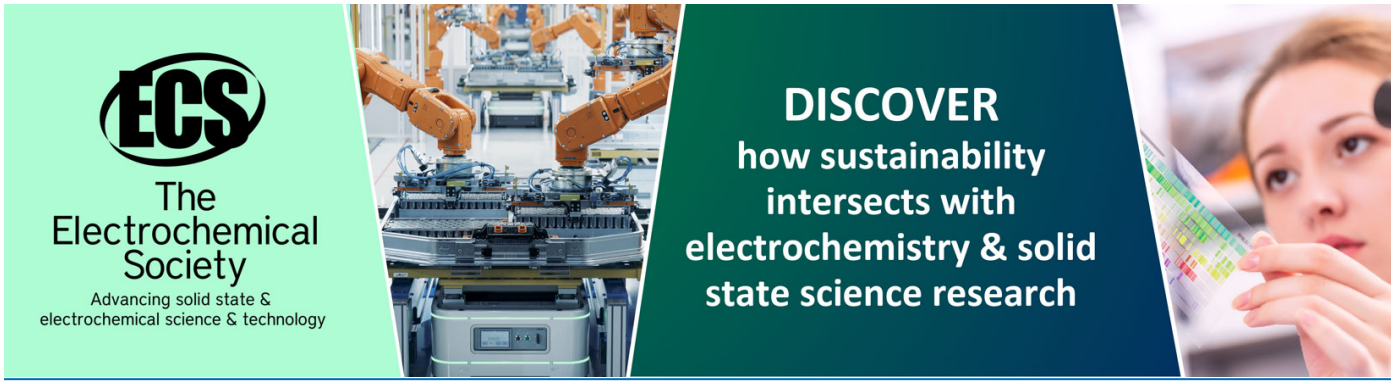

IOP Publishing Journal of Physics D: Applied Physics

J. Phys. D: Appl. Phys. **55** (2022) 034002 (16pp) https://doi.org/10.1088/1361-6463/ac292f

Polaromics: deriving polarization parameters from a Mueller matrix for quantitative characterization of biomedical specimen

Pengcheng Li[1,2], Yang Dong[1,2], Jiachen Wan[4], Honghui He[1,*], Tariq Aziz[5] and Hui Ma[1,2,3,*]

[1] Guangdong Engineering Center of Polarization Imaging and Sensing, Shenzhen Key Laboratory for Minimal Invasive Medical Technologies, Tsinghua Shenzhen International Graduate School, Tsinghua University, Shenzhen 518055, People's Republic of China
[2] Center for Precision Medicine and Healthcare, Tsinghua-Berkeley Shenzhen Institute, Shenzhen 518071, People's Republic of China
[3] Department of Physics, Tsinghua University, Beijing 100084, People's Republic of China
[4] Department of Applied Physics, New York University, Tandon School of Engineering, Brooklyn, NY, 11201, United States of America
[5] Department of Physics, Mirpur University of Science and Technology (MUST), Mirpur AJK-10250, Pakistan

E-mail: mahui@tsinghua.edu.cn and he.honghui@sz.tsinghua.edu.cn

Received 28 March 2021, revised 15 September 2021
Accepted for publication 22 September 2021
Published 18 October 2021

Abstract

A Mueller matrix is a comprehensive representation of the polarization transformation properties of a sample, encoding very rich information on the microstructure of the scattering objects. However, it is often inconvenient to use individual Mueller matrix elements to characterize the microstructure due to a lack of explicit connections between the matrix elements and the physics properties of the scattering samples. In this review, we summarize the methods to derive groups of polarization parameters, which have clear physical meanings and associations with certain structural properties of turbid media, including various Mueller matrix decomposition (MMD) methods and the Mueller matrix transformation (MMT) technique. Previously, experimentalists have chosen the most suitable method for the specific measurement scheme. In this review, we introduce an emerging novel research paradigm called 'polaromics'. In this paradigm, both MMD and MMT parameters are considered as polarimetry basis parameters (PBP), which are used to construct polarimetry feature parameters (PFPs) for the quantitative characterization of complex biomedical samples. Machine learning techniques are involved to find PFPs that are sensitive to specific micro- or macrostructural features. The goal of this review is to provide an overview of the emerging 'polaromics' paradigm, which may pave the way for biomedical and clinical applications of polarimetry.

Keywords: polarized light, Mueller matrix, polarimetry, microstructural feature, biomedicine

(Some figures may appear in colour only in the online journal)

* Authors to whom any correspondence should be addressed.

1. Introduction

Mueller polarimetry is a powerful tool for analyzing biomedical samples. The polarization state of light changes as it propagates in anisotropic media, reflected by surfaces or scattered by particles embedded in the media [1]. Therefore, polarization measurements can provide rich information about the microstructural, optical and other physics properties of the sample [2–7].

Polarization states of light can be described by a four-dimensional real number vector, called a Stokes vector $\boldsymbol{S}$. The polarization effect of the sample (assuming it is a linear transformation) can be formulated as $\boldsymbol{S}_{\text{out}} = \boldsymbol{M}\boldsymbol{S}_{\text{in}}$. The general polarization property of a sample, or the capability of a sample to alter the polarization states during the interactions, can be described by a 4×4 matrix, called a Mueller matrix $\boldsymbol{M}$ [8].

$$\boldsymbol{M} = \begin{bmatrix} m_{11} & m_{12} & m_{13} & m_{14} \\ m_{21} & m_{22} & m_{23} & m_{24} \\ m_{31} & m_{32} & m_{33} & m_{34} \\ m_{41} & m_{42} & m_{43} & m_{44} \end{bmatrix}. \tag{1}$$

The direct physical meaning of a Mueller matrix is that it is a transformation matrix of polarization states. The matrix elements represent the capability of a sample to transform between different polarization components before and after the interaction, but their relations to physical properties of the sample are often not clear. Experimentally observed values of the Mueller matrix elements contain contributions from many different factors, which include, but are not limited to, the geometrical properties of the scattering particles (size, shape, orientation and alignment), the optical properties of the scatters and the interstitial medium (complex refractive indices, diattenuation, retardance, etc), the thickness of different layers, the orientation and the thickness of the sample.

There have been consistent efforts to develop various polarization-sensitive experimental techniques for different applications, with each technique defining its own polarization parameters. Jacques *et al* use a linearly polarized light for illumination and rotate the second polarization filter inserted in the detection arm in parallel ($I_{\parallel}$) and perpendicular ($I_{\perp}$) configurations. The degree of linear polarization (Pol or LDOP) has been used as a polarization parameter to enhance the contrast between healthy and cancerous regions in skin pathologies [9, 10]. Oldernburg *et al* designed the polarized light microscope (named PolScope) which can measure the linear retardance of the sample and the orientation of the slow axis [11, 12].

For anisotropic samples, the LDOP parameter is sensitive to the sample orientation. Zeng *et al* defined a new set of polarization parameters by measuring all linear polarization directions and fitting a sinusoidal curve [13]. Later, this method was further improved and named the rotating linear polarization imaging (RLPI) technique [14]. The polarization parameters provided by RLPI include the G and $\varphi_3/2$, which are related to the anisotropy and the orientation of anisotropy of the sample. All these parameters can be expressed as functions of the Mueller matrix elements. (Details of the parameters will be listed in the appendix.)

Another way to extract information with clear physical meanings from the Mueller matrix is the Mueller matrix decomposition (MMD) techniques, which represent the nonlinear data compression algorithms. Lu and Chipman [15] proposed the Mueller matrix polar decomposition (MMPD) method which approximates a complex medium to a layered structure, decompoing the Mueller matrix into the product of diattenuation, retardation and depolarization matrices. MMPD can provide parameters including diattenuation, polarizance, retardance, optical rotation and depolarization, all of which can be expressed as functions of Mueller matrix elements [16]. The technique has been proved effective in various biomedical and clinical applications, such as the detection and staging of liver cancer [17, 18], breast cancer [19, 20], cervical cancer [21–24], colon cancer [25–29], inflammatory bowel diseases [30], Alzheimer's disease [31], gastric cancer [32], and so on [33–37].

However, the MMPD method assumes that the order of three polarization effects follows: diattenuation first, retardance second, general depolarization last. A different ordering of these three components might affect the accuracy of the decomposed results due to the noncommutating property of matrix multiplication. Ghosh *et al* compared different orderings of decomposition and showed that the order chosen in Lu–Chipman decomposition is suitable for biomedical studies [38]. Li *et al* carried out Monte Carlo simulations of a layered cylinder-birefringent model and showed that Lu–Chipman decomposition is applicable to a homogeneous or layered sample with correct order, and errors occur for a layered sample with a reversed order [39].

Ossikovski [40] and Ortega-Quijano *et al* [41, 42] proposed the differential method to separate depolarization and pure polarization effects, which assumes not the order of these effects, but that the medium is longitudinally continuous and homogeneous. Details of these parameters will be discussed in section 2.

Intrigued by RLPI and MMD, He *et al* proposed the Mueller matrix transformation (MMT) concept [43]: using different techniques to transform the Mueller matrix elements to polarization parameters to characterize specific microstructural features or optical and other physics properties of the samples. These parameters can be identified by examining or fitting data from experiments or Monte Carlo (MC) simulations. Some recent comparative studies showed that the MMT and MMPD parameters have different advantages for different applications [44–46].

Following the work by Gil on the invariant parameters in a Mueller matrix under rotation and retarder transformation [47], Li *et al* studied the rotation and mirror symmetry properties of the sample [48], and derived a set of polarization parameters which are invariant to random azimuth orientations, and also provide a set of corresponding orientation parameters [48]. They further studied four types of Mueller matrix transformations (rotation, reciprocal, longitudinal mirror and transverse mirror) and corresponding symmetries, and derived parameters that are sensitive to the layered

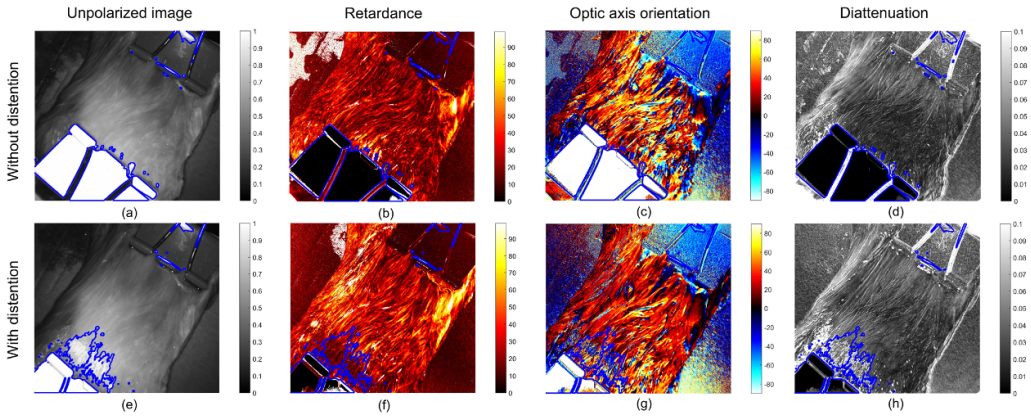

Figure 1. Unpolarized image, retardance image, optic axis orientation map, and diattenuation images of the bladders, acquired using polarimetric endoscope [57].

structure [39]. Details of these parameters will be shown in the appendix.

In a recent attempt [49], polarization parameters from MMD and MMT are used as polarimetry basis parameters (PBPs). With the help of machine learning, new polarimetry feature parameters (PFPs) are derived which are more sensitive to specific pathological structures and can quantitatively characterize histological slices in biomedical applications.

Meanwhile, more and more Mueller matrix polarimetric imaging equipment has been developed for various biomedical and clinical studies and applications, such as transmission and reflection Mueller matrix microscopes [17, 50–52], the Mueller matrix mesoscope [53], the Mueller matrix colposcope [54, 55], and several different types of Mueller matrix endoscope [56–60]. An example is shown in figure 1. Polarization measurements can also combine with other optical modalities [61–63].

In the following sections of this review, we present more details to summarize the consistent efforts to derive polarization parameters which are sensitive to specific micro- or macro-structural features and optical or other physics properties of turbid media.

2. Mueller matrix decomposition methods

The concept of Mueller matrix decomposition is simple: changes in polarization states during the propagation of polarized light in a complex scattering sample can be regarded as the combined effects of several known physics processes which affect polarization, i.e. retardation, diattenuation and depolarization. Therefore, a Mueller matrix can be decomposed to derive parameters which characterize the contributions by these physics processes, such as retardance, dichroism and depolarization coefficients.

There are three types of Mueller matrix decomposition method: product decomposition, sum decomposition and combined serial-parallel decompositions [64]. The product decomposition assumes that when light passes through the media, the polarization effects occur in serial order. Therefore product decompositions are suitable for a sample with a layered structure, or polarization effects occur with serial order. The sum decomposition, which assumes the polarization effects occur in parallel in the media, is suitable for analyzing transversely inhomogeneous samples. In biomedical studies, the optical model could be complicated, and decomposing an optical sample would be like guessing a circuit in a black box and trying decompose it with a suitable series-parallel model.

2.1. Lu–Chipman decomposition

Lu–Chipman decomposition, or Mueller matrix polar decomposition (MMPD) [15], is one of the most commonly used product decomposition methods in biomedical studies. It assumes the optical effects in the sample are serial, and follow the order as diattenuation, retardation and general depolarization (general means this component also includes the polarizance effect).

$$\begin{aligned}\boldsymbol{M} &= m_{11}\begin{bmatrix}1 & \boldsymbol{D}^{\mathsf{T}}\\ \boldsymbol{P} & \boldsymbol{m}_{3\times3}\end{bmatrix} = \boldsymbol{M}_{\Delta}\boldsymbol{M}_{\mathrm{R}}\boldsymbol{M}_{\mathrm{D}}\\ &= \begin{bmatrix}1 & \boldsymbol{0}^{\mathsf{T}}\\ \boldsymbol{P}_{\Delta} & \boldsymbol{m}_{\Delta}\end{bmatrix}\begin{bmatrix}1 & \boldsymbol{0}^{\mathsf{T}}\\ \boldsymbol{0} & \boldsymbol{m}_{\mathrm{R}}\end{bmatrix}\begin{bmatrix}1 & \boldsymbol{D}^{\mathsf{T}}\\ \boldsymbol{D} & \boldsymbol{m}_{\mathrm{D}}\end{bmatrix}.\end{aligned} \tag{2}$$

The MMPD method can provide the following parameters.

First, from the first row of the Mueller matrix one can get the diattenuation vector $\boldsymbol{D}$ and its magnitude D:

$$D = \frac{1}{m_{11}}\sqrt{m_{12}^2 + m_{13}^2 + m_{14}^2}. \tag{3}$$

Then using formulae (4) and (5) we can construct the diattenuation matrix $\boldsymbol{M}_{\mathrm{D}}$

$$\boldsymbol{M}_{\mathrm{D}} = m_{11}\begin{bmatrix}1 & \vec{D}^{\mathsf{T}}\\ \vec{D} & \boldsymbol{m}_{\mathrm{D}3\times3}\end{bmatrix} \tag{4}$$

$$\boldsymbol{m}_{\mathrm{D}3\times3} = \sqrt{1-D^2}\boldsymbol{I}_3 + (1-\sqrt{1-D^2})\hat{\boldsymbol{D}}\hat{\boldsymbol{D}}^{\mathsf{T}}. \tag{5}$$

We decompose $\boldsymbol{M}_{\mathrm{D}}$ from the original Mueller matrix $\boldsymbol{M}' \equiv \boldsymbol{M}\boldsymbol{M}_{\mathrm{D}}^{-1}$, and by the assumption in equation (2), this matrix is the product of the retardance matrix and the depolarization matrix:

$$\begin{bmatrix} 1 & \mathbf{0}^{\mathsf{T}} \\ \boldsymbol{P}_{\Delta} & \boldsymbol{m}_{\Delta} \end{bmatrix} \begin{bmatrix} 1 & \mathbf{0}^{\mathsf{T}} \\ \mathbf{0} & \boldsymbol{m}_{\mathrm{R}} \end{bmatrix} = \begin{bmatrix} 1 & \mathbf{0}^{\mathsf{T}} \\ \boldsymbol{P}_{\Delta} & \boldsymbol{m}_{\Delta}\boldsymbol{m}_{\mathrm{R}} \end{bmatrix} = \boldsymbol{M}\boldsymbol{M}_{\mathrm{D}}^{-1} \tag{6}$$

where $\boldsymbol{P}_{\Delta}$ is the polarizance vector. The matrix $\boldsymbol{M}_{\Delta}$ is called general depolarization matrix. $\boldsymbol{P}_{\Delta}$ is extracted from the first column of $\boldsymbol{M}'$. The formula to calculate $\boldsymbol{P}_{\Delta}$ from $\boldsymbol{M}$ is:

$$\boldsymbol{P}_{\Delta} = \frac{\boldsymbol{P} - \boldsymbol{m}_{3\times 3}\boldsymbol{D}}{1 - D^2}. \tag{7}$$

In the second step, we need to decompose a 3×3 matrix $\boldsymbol{m}' = (\boldsymbol{m}_{\Delta}\boldsymbol{m}_{\mathrm{R}})$. Since $\boldsymbol{m}_{\mathrm{R}}$ is a rotation transformation matrix, we can use a polar decomposition algorithm to diagonalize $\boldsymbol{m}'$. After the diagonalization, we define parameter Δ for characterizing the degree of total depolarization:

$$\Delta = 1 - \frac{1}{3}\left|\mathrm{tr}\boldsymbol{m}_{\Delta}\right| \in [0,1]. \tag{8}$$

Parameter Δ is a scalar, with value 0 representing nondepolarizing media, and value 1 representing totally depolarized media.

In the last step, we can extract retardance information from $\boldsymbol{M}_{\mathrm{R}}$. In the paper by Lu and Chipman, the formula for retardance is:

$$\cos R = \frac{1}{2}\mathrm{tr}\boldsymbol{M}_{\mathrm{R}} - 1. \tag{9}$$

In fact, parameter R contains both linear retardance and circular retardance (aka. optical rotation) effects: $\cos R = 2\cos^2(\alpha)\cos^2(\delta/2) - 1$. To decompose the linear retardance angle δ and the optical rotation angle α , we can use these formulas [65, 66]:

$$\cos\delta = \sqrt{(M_{R22} + M_{R33})^2 + (M_{R32} - M_{R23})^2} - 1 \tag{10}$$

$$\tan\alpha = \frac{M_{R32} - M_{R23}}{M_{R22} + M_{R33}}. \tag{11}$$

When the determinant of the Mueller matrix is negative, which may occur for large size scatterers (Mie scattering) [68] or strongly depolarizing media [67] measured in reflection configuration, the MMPD algorithm needs to add 'sign factors' [67, 69] to ensure the MMPD method is still applicable. Figure 2 shows that by using the generalized MMPD method, the continuity of the image is locally preserved.

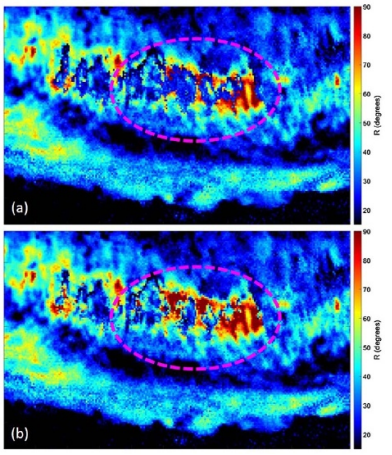

Figure 2. Retardance R images of an *ex vivo* human cervix measured in back-reflection, obtained from the (a) standard and (b) generalized procedures for decomposing negative-determinant Mueller matrices [67].

2.2. Differential decomposition

Differential decomposition is a special type of product decomposition, called continuous product decomposition [64]. It does not assume a layer media for the polarization effects occur in order, but assumes samples to be longitudinally homogeneous. Therefore, the differential decomposition method is suitable for analyzing the thickness dependence of a Mueller matrix.

To obtain optical parameters using the differential method, we first compute the logarithm matrix $\boldsymbol{L}$ of the Mueller matrix:

$$\boldsymbol{L} \equiv \ln\boldsymbol{M}. \tag{12}$$

Then we separate $\boldsymbol{L}$ to transpose the symmetric part and the anti-symmetric part $\boldsymbol{L} = \boldsymbol{L}_{\mathrm{m}} + \boldsymbol{L}_{\mathrm{u}}$ by metric $\boldsymbol{G} = \mathrm{diag}(1,-1,-1,-1)$:

$$\boldsymbol{L}_{\mathrm{m}} = \frac{1}{2}(\boldsymbol{L} - \boldsymbol{G}\boldsymbol{L}^{\mathsf{T}}\boldsymbol{G}) = \langle\boldsymbol{m}\rangle z \tag{13}$$

$$\boldsymbol{L}_{\mathrm{u}} = \frac{1}{2}(\boldsymbol{L} + \boldsymbol{G}\boldsymbol{L}^{\mathsf{T}}\boldsymbol{G}) = \frac{1}{2}\langle\Delta\boldsymbol{m}^2 z^2\rangle. \tag{14}$$

Formula (14) is an approximation, and is only strictly equal when $\langle\boldsymbol{m}\rangle$ and $\langle\Delta\boldsymbol{m}^2\rangle$ commute [70].

From the above formula we learn that pure polarization parameters in $\boldsymbol{L}_{\mathrm{m}}$ vary linearly with sample thickness, and depolarization parameters in $\boldsymbol{L}_{\mathrm{u}}$ will vary parabolically with thickness. The physical meaning for the parameters are:

$$\boldsymbol{L}_{\mathrm{m}} = \begin{bmatrix} 0 & \mathrm{LD} & \mathrm{LD}_{45} & \mathrm{CD} \\ \mathrm{LD} & 0 & \mathrm{CB} & -\mathrm{LB}_{45} \\ \mathrm{LD}_{45} & -\mathrm{CB} & 0 & \mathrm{LB} \\ \mathrm{CD} & \mathrm{LB}_{45} & -\mathrm{LB} & 0 \end{bmatrix} \tag{15}$$

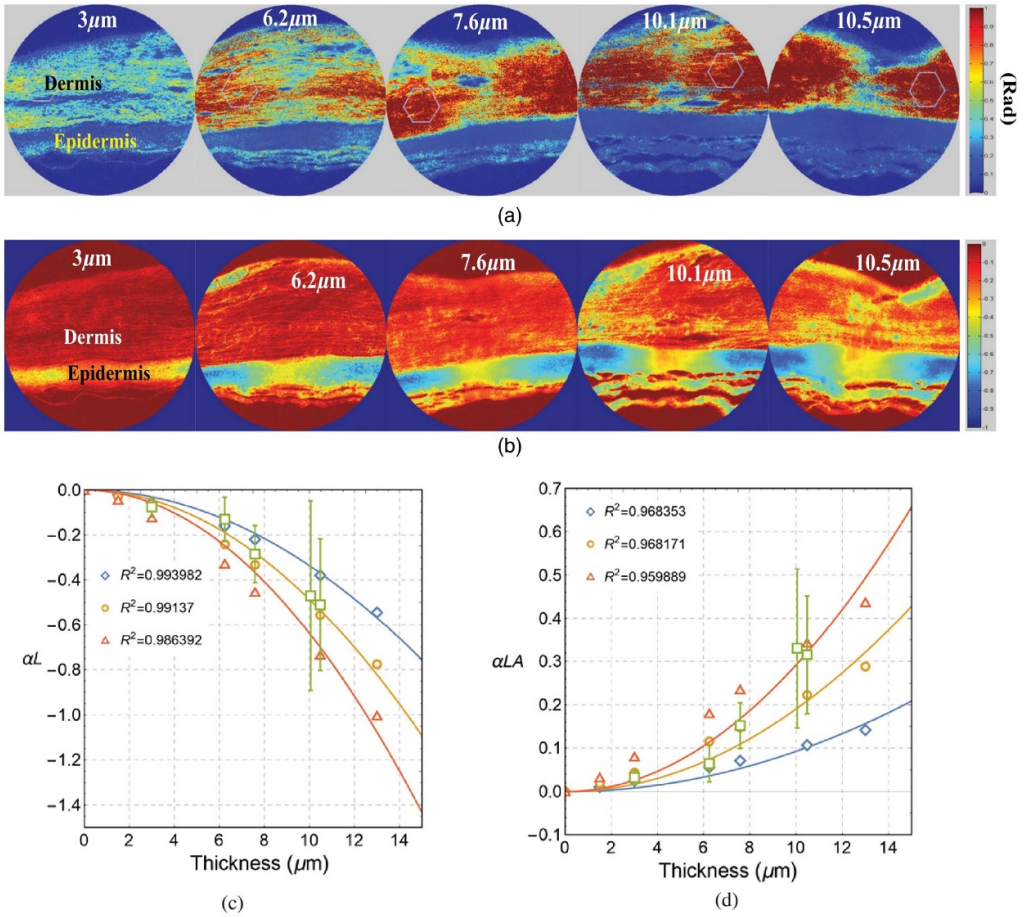

Figure 3. Maps of (a) total linear retardance and (b) depolarization coefficient α_{22} of unstained histological cuts of human skin models of different thicknesses [72]. Monte Carlo simulation of sphere-cylinder-birefrigence model matched with the experiment data, both (c) α_{L} and (d) α_{LA} vary parabolically with the thickness of the sample [71].

where LD is 0–90 deg linear diattenuation, LD_{45} is ±45 deg linear diattenuation, LB is linear birefringence, CD is circular diattenuation, CB is circular birefringence (optical rotation).

Usually we also need to subtract the effect of isotropic absorption from the diagonal elements of $\boldsymbol{L}_{\mathrm{u}}$. Take the decomposition of pure linear diattenuation as an example, the logarithm decomposition of $\boldsymbol{M}_{\mathrm{D}}(p_x, p_y)$ is:

$$\boldsymbol{L} = \boldsymbol{L}_{\mathrm{m}} + \boldsymbol{L}_{\mathrm{u}} = \begin{bmatrix} 0 & \ln(p_x/p_y) & 0 & 0 \\ \ln(p_x/p_y) & 0 & 0 & 0 \\ 0 & 0 & 0 & 0 \\ 0 & 0 & 0 & 0 \end{bmatrix} + \ln(p_x p_y)\boldsymbol{I}_4. \tag{16}$$

After subtracting isotropic absorption from $\boldsymbol{L}_{\mathrm{u}}$, we get $\boldsymbol{L}'_{\mathrm{u}} = \boldsymbol{L}_{\mathrm{u}} - L_{\mathrm{u}11}\boldsymbol{I}_4 = \boldsymbol{0}$, which means the pure linear diattenuator does not contain a depolarization effect.

The study of $\boldsymbol{L}_{\mathrm{u}}$ mainly focuses on the diagonal elements $\alpha_{ii} = L_{\mathrm{u}ii}$, where $\alpha_{22}, \alpha_{33}, \alpha_{44}$ represent 0–90 deg linear depolarization, ±45 deg linear depolarization and circular depolarization, respectively. For the physically realizable Mueller matrices, we always have $\alpha_{ii} \leqslant 0$, the lower value representing a stronger depolarization effect. Since α_{22}, α_{33} are not invariant under azimuth rotation of the sample, Li *et al* also proposed invariant parameters α_{L} and α_{LA}, representing linear depolarization and anisotropic linear depolarization, respectively [71]. These parameters are helpful for identifying the proper model for a human skin sample, as shown in figure 3.

2.3. Cloude decomposition

Cloude decomposition [73, 74] is a commonly used sum decomposition method in the studies of Mueller polarimetry. It decomposes the Mueller matrix into the sum of up to four nondepolarizing Mueller matrices. The algorithm is as follows:

First, use Pauli matrices $\boldsymbol{\sigma}_i$ to map the Mueller matrix to a Hermite matrix $\boldsymbol{H}(\boldsymbol{M})$ called a covariance matrix [74]:

$$\boldsymbol{H}(\boldsymbol{M}) = \frac{1}{4}\sum_{i,j=1}^{4} m_{ij}\boldsymbol{\sigma}_i \otimes \boldsymbol{\sigma}_j. \tag{17}$$

Hence, the eigenvalues of $\boldsymbol{H}$ are real numbers. We arrange them in descending order, $\lambda_1 \geqslant \lambda_2 \geqslant \lambda_3 \geqslant \lambda_4 \geqslant 0$. These eigenvalues contain information about the depolarization of the sample. For instance, for any nondepolarizing Mueller matrix we have $\lambda_{1\sim4} = 1, 0, 0, 0$ [75]. More than one nonzero

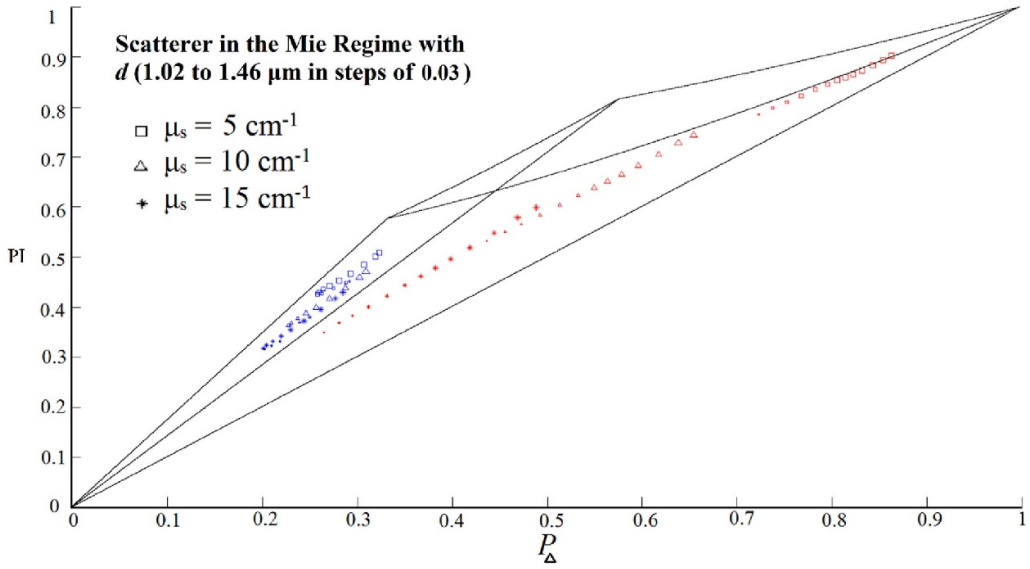

Figure 4. Spaces that physically realizable Mueller matrices could occur on the PI–P_Δ plane. Data points are generated by MC simulations of spherical scatterers in the Mie regime in forward- (red points) and back-scattering (blue points). The size of the scatterer varies from 1.02 to 1.46 μm in steps of 0.03. The increase in the size of the scatterer is shown by increasing the size of the points. μ_s is the scattering coefficient.

eigenvalue representings the Mueller matrix contains depolarization:

$$\boldsymbol{H}(\boldsymbol{M}) = \frac{1}{m_{11}} \sum_{i=1}^{4} \lambda_i \boldsymbol{H}_i \,, \quad \boldsymbol{H}_i \equiv m_{11}(\boldsymbol{u}_i \otimes \boldsymbol{u}_i^{\dagger}). \tag{18}$$

$\boldsymbol{H}_i$ are the matrices recovered from the corresponding λ_i and outer product of eigen vector $\boldsymbol{u}_i$. Since $\boldsymbol{H}_i$ are rank 1, this means we have decomposed the Mueller matrix into up to four nondepolarizing Mueller matrices. This method is called Cloude decomposition [73] or spectral decomposition [64]. Usually λ_i is between $[0,1]$, and a completely depolarizing sample has $\lambda_{1\sim4} = 1,1,1,1$. All $\lambda_i \geqslant 0$ is the condition for a physical realizable Mueller matrix [74].

Researchers also recombined λ_i into various polarization parameters, such as polarization entropy [76, 77]

$$S(\boldsymbol{H}) = -\sum_{i=1}^{4} (\lambda_i \log_4 \lambda_i) \quad (\lambda_i \,\text{are normalized by}\, m_{11}) \tag{19}$$

and indices of polarimetric purity (IPP) [78, 79]:

$$P_1 = \frac{\lambda_1 - \lambda_2}{m_{11}}, P_2 = \frac{\lambda_1 + \lambda_2 - 2\lambda_3}{m_{11}}, P_3 = \frac{\lambda_1 + \lambda_2 + \lambda_3 - 3\lambda_4}{m_{11}}. \tag{20}$$

Based on IPPs, researchers proposed the depolarization index [80]

$$P_\Delta = \sqrt{\frac{1}{3}\left(2P_1^2 + \frac{2}{3}P_2^2 + \frac{1}{3}P_3^2\right)} \tag{21}$$

and overall purity index [81]:

$$\mathrm{PI} = \sqrt{(P_1^2 + P_2^2 + P_3^2)/3} \tag{22}$$

so that we can analyze the depolarization condition of the data on a 2D plot [81, 82]. For example, on the PI–P_Δ plot, nondepolarizing data points lie at coordinate $(1,1)$, totally depolarized samples lie at $(0,0)$. Data points of physically realizable Mueller matrices lie in an approximately polygon region, shown in figure 4. Different subregions are associated with different types of depolarizations, and corresponding to different type of scatterers. A subregion occupied by the blue points, which people used to believe should be empty, is discovered that corresponds to Mie scatterers measured in the reflection configuration [81].

2.4. Summary

Mueller matrix decomposition methods usually derive several polarization parameters from the elements, meaning that they can be regarded as a kind of data compression technique. In this procedure, the feature information that researchers are interested in are extracted from the Mueller matrix, providing indicators that are easier for researchers and pathologists to grasp, thus making it easier for them to examine biomedical samples. Different MMD algorithms correspond to different optical models. The Lu–Chipman method is suitable for a homogeneous or layered sample with correct order. It can be applied in both transmission and reflection configurations, but for Mie scattering dominant samples measured in the reflection configuration we need to modify the algorithm. The differential method assumes the media is longitudinally homogeneous, usually applicable in transmission configuration. The Cloude decomposition has a wide range of applications. It can be used in both transmission and reflection configurations, and

Mie or Rayleigh scattering are both applicable and can be identified.

Currently, the Mueller matrix decomposition methods are prevalent in biomedical studies and applications for quantitative information acquisition. Generally, the decomposition methods are all based on specific models, which also bring specific limitations for application schemes. Meanwhile, the data compression procedures mean that the decomposition methods may result in a loss of detailed information contained in the Mueller matrix.

3. Mueller matrix transformation methods

In a different approach, a Mueller matrix transformation (MMT) was proposed to explain experimental data [43]. The development of MMT starts with the study of rotation and mirror transformation and symmetry properties of the sample, which lead to polarization parameters that are invariant to the azimuth orientation of the sample [48], or indicate breaking of mirror symmetries in the sample structure [39]. In fact, MMT can be considered as a more general concept which encompasses MMD, since both MMD and MMT aim to 'transform' Mueller matrix data into new polarization parameters which characterize certain physical properties of the media.

3.1. Transformations and symmetries of the Mueller matrix

There are four types of symmetries that need to be considered in the light scattering theory: rotation, reciprocal, longitudinal and transversal mirror transformation [83].

The Mueller matrix of sample $\boldsymbol{M}$ after rotation around the z-axis (which coincides with the direction of collinear illumination and detection) for α angle is $\boldsymbol{M}' = \boldsymbol{R}(\alpha)\boldsymbol{M}\boldsymbol{R}(-\alpha)$, where

$$\boldsymbol{R}(\alpha) = \begin{bmatrix} 1 & 0 & 0 & 0 \\ 0 & \cos(2\alpha) & -\sin(2\alpha) & 0 \\ 0 & \sin(2\alpha) & \cos(2\alpha) & 0 \\ 0 & 0 & 0 & 1 \end{bmatrix}. \tag{23}$$

Letting $\boldsymbol{M}' = \boldsymbol{M}$ we can deduce the Mueller matrix that is invariant under α rotation. For a sample that is invariant under 90° rotation, its Mueller matrix is $\boldsymbol{M}_{R_{90}}$:

$$\boldsymbol{M}_{R_{90}} = \begin{bmatrix} m_{11} & 0 & 0 & m_{14} \\ 0 & m_{22} & m_{23} & 0 \\ 0 & m_{32} & m_{33} & 0 \\ m_{41} & 0 & 0 & m_{44} \end{bmatrix}. \tag{24}$$

A sample that is invariant under α rotation ($\alpha \neq n\frac{\pi}{2}, n \in \mathbb{Z}$) obeys the following form:

$$\boldsymbol{M}_R = \begin{bmatrix} m_{11} & 0 & 0 & m_{14} \\ 0 & b & \beta & 0 \\ 0 & -\beta & b & 0 \\ m_{41} & 0 & 0 & m_{44} \end{bmatrix} \tag{25}$$

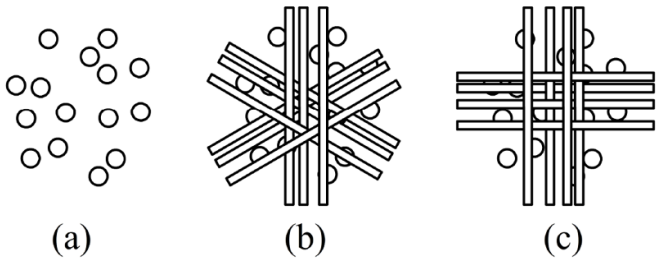

Figure 5. Different types of rotation symmetries illustrated with a scattering medium consist of spherical and cylindrical scatterers. (a) A cloud of randomly distributed spherical scatterers. (b) Mixing of three groups of cylindrical scatterers, invariant under 60° rotation. (c) Mixing of two groups of cylindrical scatterers lying orthogonal to each other, invariant under 90° rotation. It is verified with MC simulation that model (a), (b) obey form $\boldsymbol{M}_R$ and model (c) obeys form $\boldsymbol{M}_{R_{90}}$ [39].

where

$$b \equiv \frac{1}{2}(m_{22} + m_{33}) \tag{26}$$

$$\beta \equiv \frac{1}{2}(m_{23} - m_{32}). \tag{27}$$

The 'longitudinal mirror' transformation is a spatial reflection against a mirror plane defined by the illumination and detection light beams. The Mueller matrix of sample $\boldsymbol{M}$ after mirror transformation by such a plane is $\boldsymbol{M}' = \boldsymbol{H}\boldsymbol{M}\boldsymbol{H}$ [48], where $\boldsymbol{H} = \mathrm{diag}(1, 1, -1, -1)$. Letting $\boldsymbol{M}' = \boldsymbol{M}$ we can deduce that the form of a longitudinal mirror symmetric Muller matrix is:

$$\boldsymbol{M}_{H_0} = \left[\begin{array}{cc:cc} m_{11} & m_{12} & 0 & 0 \\ m_{21} & m_{22} & 0 & 0 \\ \hdashline 0 & 0 & m_{33} & m_{34} \\ 0 & 0 & m_{43} & m_{44} \end{array}\right]. \tag{28}$$

The reciprocal transformation rotates the sample around the bisectrix [83] for 180°. The reciprocal transformation of the Mueller matrix is $\boldsymbol{M}' = \boldsymbol{X}\boldsymbol{M}^{\mathsf{T}}\boldsymbol{X}$, where $\boldsymbol{X} = \mathrm{diag}(1, 1, -1, 1)$ [64]. The reciprocal symmetric Mueller matrix obeys the form:

$$\boldsymbol{M}_X = \begin{bmatrix} m_{11} & m_{12} & m_{13} & m_{14} \\ m_{12} & m_{22} & m_{23} & m_{24} \\ -m_{13} & -m_{23} & m_{33} & m_{34} \\ m_{14} & m_{24} & -m_{34} & m_{44} \end{bmatrix}. \tag{29}$$

The transverse mirror transformation uses the bisectrix plane as the mirror plane. (When the illumination and detection light path are collinear, the bisectrix plane is the xOy plane.) The transverse mirror transformation of a sample

is $\boldsymbol{M}' = \boldsymbol{T}\boldsymbol{M}^{\mathrm{T}}\boldsymbol{T}$, where $\boldsymbol{T} = \mathrm{diag}(1,1,1,-1)$. The transversal mirror symmetric Mueller matrix obeys the form:

$$\boldsymbol{M}_{\mathrm{T}} = \begin{bmatrix} m_{11} & m_{12} & m_{13} & m_{14} \\ m_{12} & m_{22} & m_{23} & m_{24} \\ m_{13} & m_{23} & m_{33} & m_{34} \\ -m_{14} & -m_{24} & -m_{34} & m_{44} \end{bmatrix}. \tag{30}$$

3.2. Mueller matrix rotation invariant parameters

There have been many studies on Mueller matrix invariant parameters. Pravdin *et al* studied the rotation invariants in both transmission and reflection Mueller matrices, and mapped the orientation of the anisotropy [84]. Gil [47] studied both rotation transformation and retarder transformation of the Mueller matrix on one side or dual sides, and proposed a corresponding set of invariants. Jiang *et al* developed the RLPI technique to reduce the orientation influence of the experimental data, and proposed a few invariant parameters and orientation parameters. To extend the RLPI technique to the full Mueller matrix, He *et al* studied the MC simulation and experimental data of a concentric silk coil and proposed the Mueller matrix transformation theory [43]. Li *et al* compared these studies together with the rotation and mirror transformation theory of the Mueller matrix, and proposed a set of commonly used rotation invariants and orientation parameters:

Given the experimental setup, if the illumination beam and the detection orientation are collinear, then we have the following Mueller matrix parameters as invariants under azimuth rotation:

$$m_{11} \tag{31}$$

$$k_{\mathrm{C}} = m_{44} \in [-1,1] \tag{32}$$

$$D_{\mathrm{C}} = m_{14} \in [-1,1] \tag{33}$$

$$P_{\mathrm{C}} = m_{41} \in [-1,1] \tag{34}$$

$$P_{\mathrm{L}} = \sqrt{m_{21}^2 + m_{31}^2} \in [0,1] \tag{35}$$

$$D_{\mathrm{L}} = \sqrt{m_{12}^2 + m_{13}^2} \in [0,1] \tag{36}$$

$$q_{\mathrm{L}} = \sqrt{m_{42}^2 + m_{43}^2} \in [0,1] \tag{37}$$

$$r_{\mathrm{L}} = \sqrt{m_{24}^2 + m_{34}^2} \in [0,1]. \tag{38}$$

Denoting the central 2×2 block of the Mueller matrix as $\boldsymbol{B}$, we also have its trace, determinant, and Frobenius norm as rotation invariants:

$$\mathrm{tr}\boldsymbol{B} = m_{22} + m_{33} = 2b \tag{39}$$

$$|\boldsymbol{B}| = (m_{22}m_{33} - m_{23}m_{32}) \tag{40}$$

$$\|\boldsymbol{B}\| = \sqrt{m_{22}^2 + m_{33}^2 + m_{23}^2 + m_{32}^2}. \tag{41}$$

However, the set $\{\mathrm{tr}\,\boldsymbol{B}, |\boldsymbol{B}|, \|\boldsymbol{B}\|\}$ is not as commonly used as another equivalent set, $\{b, \beta, t_1\}$, by experimentalists [48], where

$$b = \frac{1}{2}(m_{22} + m_{33}) \tag{42}$$

$$\beta = \frac{1}{2}(m_{23} - m_{32}) \tag{43}$$

$$t_1 = \sqrt{\tilde{b}^2 + \tilde{\beta}^2} = \frac{1}{2}\sqrt{(m_{22} - m_{33})^2 + (m_{23} + m_{32})^2}. \tag{44}$$

Parameter b is sensitive to subwavelength particle scattering, β is related to optical rotation and the coexistence of multiple anisotropic effects [48], t_1 represents the overall degree of anisotropy [43].

3.3. Mueller matrix azimuth orientation parameters

When the sample has a mirror symmetry plane (such as a sample with only one type of anisotropy effect), the Mueller matrix of the sample can be block-diagonized at a specific azimuth orientation:

$$\boldsymbol{M}_{\mathrm{mirsym}} = \left[\begin{array}{cc:cc} m_{11} & m_{12} & 0 & 0 \\ m_{21} & m_{22} & 0 & 0 \\ \hdashline 0 & 0 & m_{33} & m_{34} \\ 0 & 0 & m_{43} & m_{44} \end{array}\right]. \tag{45}$$

Thus, for a randomly oriented sample, we can extract the information of the azimuth orientation α of the anisotropy from the measured $\boldsymbol{M}'_{\mathrm{mirsym}}$

$$\begin{aligned} \boldsymbol{M}'_{\mathrm{mirsym}} &= \boldsymbol{R}(\alpha)\boldsymbol{M}_{\mathrm{mirsym}}\boldsymbol{R}(-\alpha) \\ &= \left[\begin{array}{c:ccc} m_{11} & m_{12}c_2 & m_{12}s_2 & 0 \\ \hdashline m_{21}c_2 & b + \tilde{b}c_4 & \tilde{b}s_4 & -m_{34}s_2 \\ m_{21}s_2 & \tilde{b}s_4 & b - \tilde{b}c_4 & m_{34}c_2 \\ \hdashline 0 & -m_{43}s_2 & m_{43}c_2 & m_{44} \end{array}\right] \end{aligned} \tag{46}$$

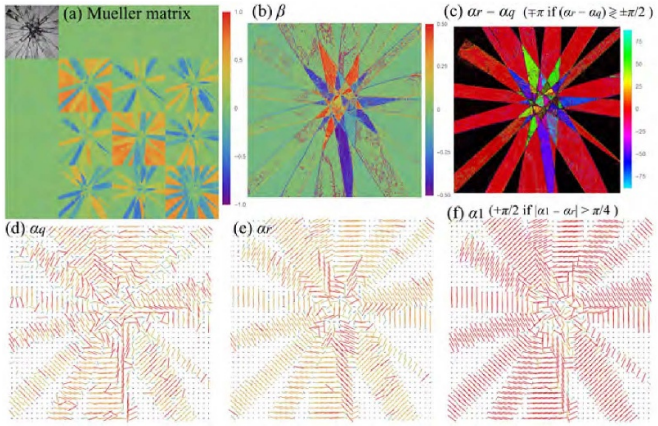

Figure 6. Measurement of transparent sticky tapes in transmission configuration. (a) The Mueller matrix, m_{11}, is plotted in $[0, 1]$ grayscale, other elements are normalized by m_{11}. (b) Invariant parameter β can show the overlapped zone of the sample. (c) The difference in orientation parameters $(\alpha_r - \alpha_q)$ can also show the overlapping of different anisotropies. (d)–(f) Orientation maps predicted by $\alpha_q, \alpha_r, \alpha_1$, length and color of the small bars represent q_L, r_L, t_1 [48].

$$c_n = \cos(n\alpha), s_n = \sin(n\alpha), \tilde{b} = \frac{1}{2}(m_{22} - m_{33}) \tag{47}$$

by using the following formulas:

$$\alpha_1 = \tfrac{1}{4}\text{atan2}(m'_{23} + m'_{32}, m'_{22} - m'_{33}) \quad \text{if } t_1 \neq 0 \tag{48}$$

$$\alpha_P = \frac{1}{2}\text{atan2}(m'_{31}, m'_{21}) \quad \text{if } P_L \neq 0 \tag{49}$$

$$\alpha_D = \frac{1}{2}\text{atan2}(m'_{13}, m'_{12}) \quad \text{if } D_L \neq 0 \tag{50}$$

$$\alpha_q = \frac{1}{2}\text{atan2}(m'_{42}, -m'_{43}) \quad \text{if } q_L \neq 0 \tag{51}$$

$$\alpha_r = \frac{1}{2}\text{atan2}(-m'_{24}, m'_{34}) \quad \text{if } r_L \neq 0. \tag{52}$$

The sign convention in equations (48)–(52) is based on the assumption that $\tilde{b}, m_{12}, m_{21}, m_{34} > 0$ and $m_{43} < 0$ when $\alpha = 0$. If the truth is the opposite, then both input parameters $(\mathrm{d}y, \mathrm{d}x)$ should flip their signs (or add π to the result of atan2). The experimental result is illustrated with a transparent sticky tapes sample, as shown in figure 6.

3.4. Mueller matrix symmetry breaking parameters

From the symmetries study of the Mueller matrix in section 3.1, one can discover that a symmetric sample can result in a transpose symmetric or antisymmetric Mueller matrix. Therefore, when analyzing a Mueller matrix whose physical structure is unknown, we can predict the types of preserved and broken symmetry in the sample by checking the indicators proposed in table 1 [39].

3.5. Summary

Similar to MMD methods, the MMT method also maps the Mueller matrix to polarization parameters with clearer physical meanings. It is a different branch of data compression techniques, or considered as a 'general MMD method'. Compared with MMD methods, there are two advantages of the MMT method: (a) the MMT method does not require the computation of the whole Mueller matrix, therefore it has better computational efficiency. (b) MMT parameters are deduced from the study of symmetries, therefore it does not pose any assumption on the optical model. It can be applied to any optical sample for both transmission and reflection configurations. The main disadvantage of the MMT method is that it is hard to find biomedical samples with perfect symmetries. Therefore, how to exploit the power of MMT parameters quantitatively remains a technical problem. In the following section, we will see a novel research paradigm called polaromics being introduced to exploit both MMD and MMT parameters quantitatively.

4. Machine leaning for polarization feature extraction

So far in this article we have summarized the consistent efforts to derive from a Mueller matrix new sets of polarization parameters which are sensitive to the intrinsic physical properties of complex samples, or orientation-sensitive parameters. These parameters include:

(a) MMD parameters, including Lu–Chipman decomposition, differential or logarithm decomposition, and Cloude decomposition.

(b) MMT parameters, including rotation invariants and orientation parameters.

In a traditional paradigm of Mueller matrix polarimetry research, experimentalists will focus on choosing the suitable MMD method according to the measurement configurations. In recent years, another research paradigm called 'polaromics' has been developed, where both MMD and MMT parameters can be taken into consideration. All the polarization parameters available are used as PBPs. Then machine learning techniques are introduced to construct PFPs for specific and quantitative characterization of micro- or macro-structural features.

For instance, in a recent attempt, Si *et al* use the correlation explanation [85] method to extract parameters that can explain the interdependence among elements [86]. The efficacy of this method was demonstrated on the classification of different morphologies of electrospun fibers.

In histopathology, biological or medical samples are routinely treated by various staining techniques to bring up selectively specific pathological features. Experienced pathologists examine the stained samples and identify areas of interest for diagnosis. By taking Mueller matrix images of the

Table 1. Mueller matrix indicators for breaking of symmetries (marked by '×'). 'DD/RR' means mixing pure LD/LR effects with a nontrivial difference angle of azimuth orientation in separated layers, 'DR2/1' means LD and LR are mixed in two layers or one layer. 'T' means true [39].

Indicator	$\boldsymbol{M}_{\mathrm{R}}$	$\boldsymbol{M}_{\mathrm{H}}$	$\boldsymbol{M}_{\mathrm{T}}$	$\boldsymbol{M}_{\mathrm{X}}$	DD	RR	DR2	DR1
$m_{22} \neq m_{33}$	×				T	T	T	T
$m_{23} = m_{32} \neq 0$	×			×				T
$m_{23} = -m_{32} \neq 0$		×	×					
$\lvert m_{23}\rvert \neq \lvert m_{32}\rvert$	×	×	×	×	T	T	T	
$m_{14} = m_{41} \neq 0$		×	×					
$m_{14} = -m_{41} \neq 0$		×		×				T
$\lvert m_{14}\rvert \neq \lvert m_{41}\rvert$		×	×	×			T	
$P_{\mathrm{L}} \neq D_{\mathrm{L}}$	×		×	×			T	
$q_{\mathrm{L}} \neq r_{\mathrm{L}}$	×		×	×			T	
$\cos\alpha_{\mathrm{PD}} \neq \pm 1$	×	×	×	×	T		T	
$\cos\alpha_{\mathrm{rq}} \neq \pm 1$	×	×	×	×		T	T	

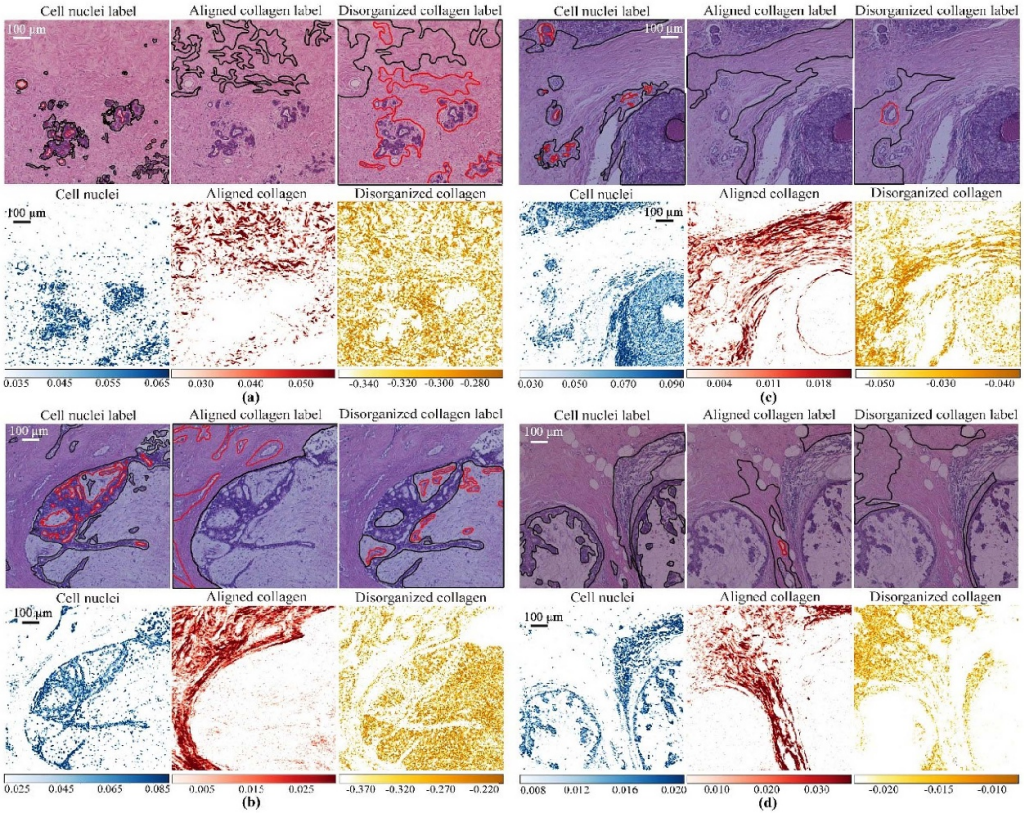

Figure 7. Quantitative characterization of cell nuclei (blue pixels), aligned collagen (red pixels), and disorganized collagen (orange pixels) using the PFPs in H&E pathological sections of different breast tissues: (a) healthy breast tissue; (b) breast fibroma; (c) breast ductal carcinoma; (d) breast mucinous carcinoma. The areas inside the black solid line contours and outside the red solid line contours in H&E images are the target microstructural features labeled by the breast pathologist. The image size is 800 × 800 pixels [49].

same sample and labeling pixels within the segmented areas, researchers can extract polarization features from Mueller matrices of all the labeled pixels using supervised learning. In the work of [49], low resolution microscopic Mueller matrix images of hematoxylin and eosin (H&E) sections are recorded from four types of typical breast tissues (TBT), i.e. healthy breast tissue, breast fibroma, breast ductal carcinoma and breast mucinous carcinoma. Based on visual inspection and segmentation of the H&E color images, pathologists can label on the polarization images areas corresponding to distinctive pathological features (DPF), i.e. cell nuclei, aligned collagen, and disorganized collagen. A group of MMT parameters are selected as the PBPs for the input data of training models, using prior knowledge on the sensitivities of these PBPs to differentiate the three types of DPFs as the criteria. Then, a supervised learning method based on linear discriminant analysis (LDA) is adopted to derive new PFPs as linear combinations of PBPs, which provide better quantitative characterization of the three DPFs in each typical breast pathological tissue, as shown in figure 7.

The training and testing of PFPs were completed in pathological samples from 32 patients. By the validation of the PFPs' performance with the corresponding H&E images as ground truth, it is concluded that: the performance of PFPs in identifying the carcinogenesis-related microstructures is satisfactory with the accuracy ranging from 0.82 to 0.91. The results demonstrate that it is viable to derive new PFPs using the simple linear combination model of PBPs and achieve a better differentiation of the DPFs from low resolution images of H&E pathological sections of different TBTs.

We believe there are many advantages of polaromics compared with the traditional data compression techniques. Polaromics examine all polarization parameters comprehensively, and provide parameters that have clearer associations with the structures that a researcher is interested in. The polaromics parameters have explicit expressions, and can therefore be easily shared compared with training neural networks or deep learning. Their explicit expressions also allow researchers to analyze the contributions from various PBPs quantitatively and improve our understanding of the relationship between physical structures and Mueller matrices.

5. Conclusions

A Mueller matrix encodes rich information on the microstructure of complex scattering samples, such as pathological specimens in clinics. However, in real biomedical applications, it is inconvenient to use the Mueller matrix directly. To deal with this problem, MMD and MMT methods have been developed to provide new polarization parameters which are sensitive to specific micro- or macro-structural features and physics properties but insensitive to the orientation of the media. For transmission configuration, MMPD is suitable for a homogeneous or layered sample with correct order, while the differential method is suitable for a longitudinally homogeneous sample measured in the transmission configuration. Cloude decomposition is widely applicable. The MMT method does not post assumptions on the optical model of the sample, and can compute faster than MMD methods. Hence the MMT method will be more suitable for fast imaging and *in vivo* measurements. Though they are prevalent techniques in biomedical and clinical applications, the MMD methods as data compression procedures based on specific optical models, or MMT methods related with specific symmetry properties, have specific limitations for real application situations. This means that we need a more thorough Mueller matrix analyzing method for information acquisition.

In recent years, a new research paradigm has emerged, where both MMD and MMT parameters can be taken into consideration (as PBPs). In the second step, based on the possible combination of PBPs, machine learning methods are involved to find better parameters that suit the experimentalist's specific tasks, known as PFPs. We call this new research paradigm of Mueller matrix polarimetry 'polaromics', which is cognate with genomics, proteomics, radiomics… etc. PBPs are the building blocks of polaromics as genes are the building blocks of genomics. Compared with the MMD and MMT methods, in polaromics machine learning add extra power to our capability to disentangle the microstructural features encoded in Mueller matrices. When a Mueller matrix image is labeled at pixel level by other imaging modalities, supervised learning can be applied to extract the corresponding polarization and microstructural features.

Polarization imaging techniques are label-free, information-rich, sensitive to subcellular features and less sensitive to imaging resolution. Among the available polarization imaging techniques, Mueller matrix polarimetry, which can provide comprehensive polarization-related structural information of media, is attracting more and more attention in biomedical studies. As summarized in this review article, PBPs derived from the traditional MMD and MMT techniques provide a more explicit description of the microstructure. Meanwhile, the fast advances in data techniques also add extra capabilities for polaromics to disentangle the microstructural features encoded in Mueller matrices. Together with the polarization optical hardware developments, and computing power enhancement, polarimetry is demonstrating greater application potential and is likely to become a powerful tool in clinical diagnosis.

Data availability statement

The data generated and/or analysed during the current study are not publicly available for legal/ethical reasons but are available from the corresponding author on reasonable request.

Acknowledgments

This work has been supported by National Natural Science Foundation of China (Grant Nos. 61527826 and 11974206), Shenzhen Bureau of Science and Innovation (Grant Nos. JCYJ20170412170814624 and JCYJ20160818143050110).

Appendix. Collection of proposed Mueller matrix parameters

Table A1. Linear polarization difference imaging parameters.

Parameter	Physical meaning
$\mathrm{LDP} = I_{\parallel} - I_{\perp}$	Linear polarization difference (historically used acronyms were DP [87], LPD [13] and LDP [14]).
$\mathrm{LDOP} = (I_{\parallel} - I_{\perp})/(I_{\parallel} + I_{\perp})$	Degree of linear polarization (Pol [9, 10] or LDOP [13]).

Table A2. Rotating linear polarization imaging (RLPI [13, 14, 87]) parameters [13, 14, 87].

Parameter	Physical meaning
$B^* = (m_{22}^2 + m_{23}^2 + m_{32}^2 + m_{33}^2)/2$	An intermediate variable, add $*$ to avoid confusion with MMT parameters. By comparing with MMT invariants we can find $B^* = \|\boldsymbol{B}\|^2/2$.
$A^* = [B^{*2} - (m_{22}m_{33} - m_{23}m_{32})^2]^{1/2}$	Anisotropy (not normalized), add $*$ to avoid confusion with MMT parameters. By comparing with MMT invariants we can find that $A^* = [\frac{1}{2}\|\boldsymbol{B}\|^4 - \|\boldsymbol{B}\|]^{1/2}$ thus it is a rotation invariant.
$G = A^*/B^*$	Anisotropy of the media [13, 14].
$C = \sqrt{m_{21}^2 + m_{31}^2}$	Anisotropy of the media, with more variation compared with A^* and B^* during RLPI experiments [14].
$\varphi_3 = \mathrm{atan}(m_{31}/m_{21})$	The orientation angle of the fibrous structure in the media (used with a factor $\varphi_3/2$) [13, 14].

Table A3. Lu–Chipman decomposition parameters [15].

Parameter	Physical meaning
$D = m_{11}^{-1}\sqrt{m_{12}^2 + m_{13}^2 + m_{14}^2}$	Degree of diattenuation.
$P = \lvert(\vec{P} - \boldsymbol{m}_{3\times3}\vec{D})/(1 - D^2)\rvert$	Degree of polarizance.
$\Delta = 1 - \frac{1}{3}\lvert\mathrm{tr}\,\boldsymbol{m}_{\Delta}\rvert \in [0, 1]$	Degree of overall depolarization. $\Delta = 0$ means nondepolarizing. $\Delta = 1$ means completely depolarized.
$\delta = \mathrm{acos}(\sqrt{(M_{R22} + M_{R33})^2 + (M_{R32} - M_{R23})^2} - 1)$	Retardation angle of linear retardance [65, 66].
$\alpha = \mathrm{atan}((M_{R32} - M_{R23})/(M_{R22} + M_{R33}))$	Angle of optical rotation (aka. circular retardance, CR) [65, 66].
$R = \frac{1}{2}\mathrm{tr}\,\boldsymbol{M}_{\mathrm{R}} - 1$	Total retardance [15]. It includes both effect of LR and CR effect [65].

Table A4. Differential decomposition parameters.

Parameter	Physical meaning
$\mathrm{LD} = \sqrt{L_{m12}^2 + L_{m13}^2}$	For pure linear diattenuation (LD) $\sqrt{L_{m12}^2 + L_{m13}^2} = \ln(p_x/p_y)$.
$\delta = \sqrt{L_{m42}^2 + L_{m43}^2}$	For pure LR this parameter is equal to retardation angle δ.
$2\alpha = L_{m23} = -L_{m32}$	For pure CR this parameter is equal to doubled optical rotation angle 2α.
$\mathrm{CD} = L_{m14} = L_{m41}$	Degree of circular diattenuation (CD).
$\alpha_{22} = L_{\mathrm{u}22}$	0–90 deg linear depolarization. Not rotation invariant.
$\alpha_{33} = L_{\mathrm{u}33}$	$\pm$45 linear depolarization. Not rotation invariant.
$\alpha_{44} = L_{\mathrm{u}44}$	Circular depolarization. Azimuth rotation invariant.
$\alpha_{\mathrm{L}} = \frac{1}{2}(\alpha_{22} + \alpha_{33}) = \frac{1}{2}(L_{22} + L_{33})$	Linear depolarization. Azimuth rotation invariant [71].
$\alpha_{\mathrm{LA}} = \frac{1}{2}\sqrt{(\alpha_{22} - \alpha_{33})^2 + (L_{\mathrm{u}23} + L_{\mathrm{u}32})^2}$	Anisotropic linear depolarization. Azimuth rotation invariant. Cylinder scatterer contribute to α_{LA}. Thin cylinder can create stronger α_{LA}. Sphere-birefringence system has no contribution to α_{LA} [71].

Table A5. Cloude decomposition parameters.

Parameter	Physical meaning
$\lambda_{1\sim4}$	Eigenvalues of the covariance matrix of MM $\boldsymbol{H}(\boldsymbol{M})$, $\lambda_1 \geqslant \lambda_2 \geqslant \lambda_3 \geqslant \lambda_4 \geqslant 0$.
$P_1 = (\lambda_1 - \lambda_2)/m_{11}$	Indices of polarimetric purity (IPP) [80].
$P_2 = (\lambda_1 + \lambda_2 - 2\lambda_3)/m_{11}$	
$P_3 = (\lambda_1 + \lambda_2 + \lambda_3 - 3\lambda_4)/m_{11}$	
$P_\Delta = \sqrt{(2P_1^2 + \frac{2}{3}P_2^2 + \frac{1}{3}P_3^2)/3}$	Depolarization index [80].
$S(\boldsymbol{H}) = -\sum_{i=1}^{4}(\lambda_i \log_4 \lambda_i)$	Polarization entropy [76].
$\mathrm{PI} = \sqrt{(P_1^2 + P_2^2 + P_3^2)/3}$	Overall purity index [81].

Table A6. MMT parameters: four 'corners' of MM.

Parameter	Physical meaning
m_{11}	Transmittance or reflectivity (depending on transmission or reflection configuration during experiment) regardless of polarization. Invariant under rotation or retarder transformation [47].
m_{14}	Associated with circular diattenuation effect. Overlapping LD following LR can also create nonzero m_{14}.
m_{41}	Associated with circular polarization effect. Overlapping LR following LD can also create nonzero m_{41}.
$\mathrm{CD} = m_{14} + m_{41}$	Degree of circular dichroism anisotropy [88].
m_{44}	m_{44} is related to many effects. For pure LR, $m_{44} = \cos\delta$. For pure LD, $m_{44} = p_x p_y$. For a pure depolarizer, m_{44} is the maintaining of circular polarization. CR has no contribution to m_{44}.

Table A7. MMT parameters: central 2×2 block of MM, where $\boldsymbol{B} = \begin{bmatrix} m_{22} & m_{23} \\ m_{32} & m_{33} \end{bmatrix}$.

Parameter	Physical meaning
$b = \frac{1}{2}(m_{22} + m_{33})$	Related to linear depolarization, also affected by LD or LR anisotropies. b is sensitive to subwavelength particles scattering.
$\beta = \frac{1}{2}(m_{23} - m_{32})$	For pure CR (optical rotation) $\beta = -\sin(2\alpha)$. The overlap of multiple linear anisotropies (LDs or LRs or both) also result in nonzero β. It is still controversial should the second case be considered as optical rotation effect.
$\tilde{b} = \frac{1}{2}(m_{22} - m_{33})$	$\tilde{b}$ is a part of anisotropy parameter t_1. Notice $\tilde{b}$ is not a rotation-invariant parameter.
$\tilde{\beta} = \frac{1}{2}(m_{23} + m_{32})$	$\tilde{\beta}$ is another part of anisotropy parameter t_1. Notice $\tilde{b}$ is not a rotation-invariant parameter.
$\lvert\boldsymbol{B}\rvert = m_{22}m_{33} - m_{23}m_{32}$	Determinant of MM central 2×2 block, affected by LD and LR but not affected by CR.
$\lVert\boldsymbol{B}\rVert = \sqrt{m_{22}^2 + m_{23}^2 + m_{32}^2 + m_{33}^2}$	Frobenius norm of MM central 2×2 block, affected by LD and LR but not affected by CR.
$t_1 = \frac{1}{2}\sqrt{(m_{22} - m_{33})^2 + (m_{23} + m_{32})^2}$	Degree of overall linear anisotropy, both LD and LR contribute to this parameter. t_1 was first proposed in [43]. By comparing with other invariants we can find that $t_1 = \frac{1}{2}\sqrt{\lVert\boldsymbol{B}\rVert^2 - 2\lvert\boldsymbol{B}\rvert}$, thus it is also an invariant. t_1 is only numerically unstable during strong absorption, thus is more stable compared with A parameter.
$A = \frac{2bt_1}{b^2 + t_1^2}$	Degree of overall linear anisotropy (normalized by b). Numerically unstable during strong absorption, strong depolarization and HWP [48], therefore not so commonly used compared with t_1 in the future.
$\alpha_1 = \frac{1}{4}\mathrm{atan2}(m'_{23} + m'_{32}, m'_{22} - m'_{33})$	Azimuth orientation of the anisotropy (not rotation invariant). α_1 has better signal-to-noise ratio but half the value range compared with other orientation parameters $(\alpha_D, \alpha_P, \alpha_q, \alpha_r)$ [89]. Since different software uses different definitions for atan2, here we point out that in this paper we follow the order $\mathrm{atan2}(\mathrm{d}y, \mathrm{d}x)$.

Table A8. MMT parameters: four 'edges' of MM.

Parameter	Physical meaning
$D_{\mathrm{L}}=\sqrt{m_{12}^2+m_{13}^2}\in[0,1]$	Linear diattenuation, sensitive to the illumination side configuration.
$P_{\mathrm{L}}=\sqrt{m_{21}^2+m_{31}^2}\in[0,1]$	Linear polarizance, sensitive to the detector side configuration.
$q_{\mathrm{L}}=\sqrt{m_{42}^2+m_{43}^2}\in[0,1]$	Capability of transforming incident circular polarization to linear polarization.
$r_{\mathrm{L}}=\sqrt{m_{24}^2+m_{34}^2}\in[0,1]$	Capability of transforming incident linear polarization to circular polarization.
$\alpha_D=\frac{1}{2}\mathrm{atan2}(m'_{13},m'_{12})$	Orientation parameter (not rotation invariant) corresponding to linear diattenuation.
$\alpha_P=\frac{1}{2}\mathrm{atan2}(m'_{31},m'_{21})$	Orientation parameter (not rotation invariant) corresponding to linear polarizance.
$\alpha_q=\frac{1}{2}\mathrm{atan2}(m'_{42},-m'_{43})$	Orientation parameter (not rotation invariant) corresponding to linear retardance.
$\alpha_r=\frac{1}{2}\mathrm{atan2}(-m'_{24},m'_{34})$	Orientation parameter (not rotation invariant) corresponding to linear retardance.

Table A9. Breaking of transpose symmetry parameters. Physical reason could be: (a) multi-layered sample overlapped, (b) nontrivial zenith angle for cylindrical scatterer or sphere-birefringence media, (c) absorption could also lead to this symmetry breaking.

Parameter	Physical meaning
$\alpha_{\mathrm{D}}-\alpha_{\mathrm{P}}$	$\alpha_{\mathrm{D}}-\alpha_{\mathrm{P}}\neq 0,\pm\frac{\pi}{2}$ shows breaking of transpose symmetry [48]. Invariant under azimuth rotation [84].
$\alpha_{\mathrm{r}}-\alpha_{\mathrm{q}}$	$\alpha_{\mathrm{r}}-\alpha_{\mathrm{q}}\neq 0,\pm\frac{\pi}{2}$ shows breaking of transpose symmetry [48]. Invariant under azimuth rotation [84].
$\cos\alpha_{\mathrm{DP}}=(m_{12}m_{21}+m_{13}m_{31})/(D_{\mathrm{L}}P_{\mathrm{L}})$	$\cos\alpha_{\mathrm{DP}}\neq\pm1$ shows breaking of transpose symmetry [39]. Invariant under azimuth rotation [84].
$\cos\alpha_{\mathrm{rq}}=(m_{24}m_{42}+m_{34}m_{43})/(r_{\mathrm{L}}q_{\mathrm{L}})$	$\cos\alpha_{\mathrm{rq}}\neq\pm1$ shows breaking of transpose symmetry [39]. Invariant under azimuth rotation [84].
$\sin\alpha_{DP}=(m_{12}m_{31}-m_{13}m_{21})/(D_{\mathrm{L}}P_{\mathrm{L}})$	Nonzero value shows breaking of transpose symmetry. Invariant under azimuth rotation [84].
$\sin\alpha_{\mathrm{rq}}=(m_{24}m_{43}-m_{34}m_{42})/(r_{\mathrm{L}}q_{\mathrm{L}})$	Nonzero value shows breaking of transpose symmetry. Invariant under azimuth rotation [84].
$\sqrt{(m_{12}-m_{21})^2+(m_{13}-m_{31})^2}$	Nonzero value shows breaking of transpose symmetry. Invariant under azimuth rotation.
$\sqrt{(m_{24}+m_{42})^2+(m_{34}+m_{43})^2}$	Nonzero value shows breaking of transpose symmetry. Invariant under azimuth rotation.
$\sqrt{D_{\mathrm{L}}^2+P_{\mathrm{L}}^2-2D_{\mathrm{L}}P_{\mathrm{L}}\cos\alpha_{\mathrm{rq}}}$	Vector difference of $\vec{D_{\mathrm{L}}}-\vec{P_{\mathrm{L}}}$. Invariant under azimuth rotation.
$\sqrt{r_{\mathrm{L}}^2+q_{\mathrm{L}}^2-2\,r_{\mathrm{L}}q_{\mathrm{L}}\cos\alpha_{\mathrm{rq}}}$	Vector difference of $\vec{r_{\mathrm{L}}}-\vec{q_{\mathrm{L}}}$. Invariant under azimuth rotation.

Table A10. Other invariant parameters of MM.

Parameter	Physical meaning
$\lvert\boldsymbol{M}\rvert$	Determinant of MM. Invariant under azimuth rotation.
$\mathrm{tr}\,\boldsymbol{M}=m_{11}+2b+m_{44}$	Trace of MM. Invariant under azimuth rotation.
$\lVert\boldsymbol{M}\rVert$	Frobenius norm of MM. When normalized by m_{11} we have $\lVert\boldsymbol{M}\rVert\in[1,4]$. $\lVert\boldsymbol{M}\rVert=4m_{11}^2$ is the necessary and sufficient condition for nondepolarizing MM [80].
$\boldsymbol{P}^{\mathsf{T}}\boldsymbol{D}$	An invariant proposed in [47].
$\boldsymbol{P}^{\mathsf{T}}\boldsymbol{m}\boldsymbol{D}$	An invariant proposed in [47].
$\boldsymbol{P}^{\mathsf{T}}\boldsymbol{m}^{\mathsf{T}}\boldsymbol{D}$	An invariant proposed in [47].

ORCID iDs

Honghui He https://orcid.org/0000-0001-7369-7433
Hui Ma https://orcid.org/0000-0001-9662-0447

References

[1] Bohren C F and Huffman D R 2008 *Absorption and Scattering of Light by Small Particles* (New York: Wiley)
[2] Alali S and Vitkin I A 2015 *J. Biomed. Opt.* **20** 061104
[3] Ghosh N and Vitkin A I 2011 *J. Biomed. Opt.* **16** 110801
[4] Tuchin V V 2016 *J. Biomed. Opt.* **21** 071114
[5] Qi J and Elson D S 2017 *J. Biophotonics* **10** 950–82
[6] Ramella-Roman J, Saytashev I and Piccini M 2020 *J. Opt.* **22** 123001
[7] He H, Liao R, Zeng N, Li P, Chen Z, Liu X and Ma H 2018 *J. Lightwave Technol.* **37** 2534–48
[8] Cloude S 2009 *Polarisation: Applications in Remote Sensing* (Oxford: Oxford University Press)
[9] Jacques S L, Roman J R and Lee K 2000 *Lasers Surg. Med.* **26** 119–29
[10] Jacques S L, Ramella-Roman J C and Lee K 2002 *J. Biomed. Opt.* **7** 329–40
[11] Oldenbourg R and Mei G 1995 *J. Microscopy* **180** 140–7
[12] Oldenbourg R 2013 *Cold Spring Harb. Protoc.* **2013** db–to078600
[13] Zeng N, Jiang X, Gao Q, He Y and Ma H 2009 *Appl. Opt.* **48** 6734–9
[14] Liao R, Zeng N, Jiang X, Li D, Yun T, He Y and Ma H 2010 *J. Biomed. Opt.* **15** 036014
[15] Lu S Y and Chipman R A 1996 *J. Opt. Soc. Am.* A **13** 1106–13
[16] Ghosh N, Wood M F and Vitkin I A 2008 *J. Biomed. Opt.* **13** 044036
[17] Wang Y, He H, Chang J, He C, Liu S, Li M, Zeng N, Wu J and Ma H 2016 *J. Biomed. Opt.* **21** 071112–071112
[18] Dubreuil M, Babilotte P, Martin L, Sevrain D, Rivet S, Le Grand Y, Le Brun G, Turlin B and Le Jeune B 2012 *Opt. Lett.* **37** 1061–3
[19] Dong Y, Qi J, He H, He C, Liu S, Wu J, Elson D S and Ma H 2017 *Biomed. Opt. Express* **8** 3643–55
[20] He C *et al* 2019 *Nat. Commun.* **10** 1–8
[21] Pierangelo A *et al* 2013 *Opt. Express* **21** 14120–30
[22] Rehbinder J, Haddad H, Deby S, Teig B, Nazac A, Novikova T, Pierangelo A and Moreau F 2016 *J. Biomed. Opt.* **21** 071113
[23] Shukla P and Pradhan A 2009 *Opt. Express* **17** 1600–9
[24] Chue-Sang J, Bai Y, Stoff S, Straton D, Ramaswamy S D and Ramella-Roman J C 2016 *J. Biomed. Opt.* **21** 071109
[25] Pierangelo A, Benali A, Antonelli M R, Novikova T, Validire P, Gayet B and De Martino A 2011 *Opt. Express* **19** 1582–93
[26] Pierangelo A, Manhas S, Benali A, Fallet C, Antonelli M R, Novikova T, Gayet B, Validire P and De Martino A 2012 *J. Biomed. Opt.* **17** 066009
[27] Novikova T, Pierangelo A, Manhas S, Benali A, Validire P, Gayet B and De Martino A 2013 *Appl. Phys. Lett.* **102** 241103
[28] Pierangelo A *et al* 2013 *J. Biomed. Opt.* **18** 046014
[29] Ahmad I, Ahmad M, Khan K, Ashraf S, Ahmad S and Ikram M 2015 *J. Biomed. Opt.* **20** 056012
[30] Liu T, Lu M, Chen B, Zhong Q, Li J, He H, Mao H and Ma H 2019 *J. Biophotonics* **12** e201900151
[31] Borovkova M, Bykov A, Popov A, Pierangelo A, Novikova T, Pahnke J and Meglinski I 2020 *Biomed. Opt. Express* **11** 4509–19
[32] Wang W, Lim L G, Srivastava S, Yan J S B, Shabbir A and Liu Q 2014 *J. Biomed. Opt.* **19** 046020
[33] Peyvasteh M *et al* 2020 *Laser Phys. Lett.* **17** 115606
[34] Borovkova M *et al* 2019 *PLoS One* **14** e0214494
[35] Phan Q H and Lo Y L 2017 *Opt. Laser Eng.* **92** 120–8
[36] Alali S, Aitken K J, Schröder A, Gribble A, Bagli D J and Vitkin I A 2014 *Biomed. Opt. Express* **5** 621–9
[37] Wood M F, Ghosh N, Wallenburg M A, Li S H, Weisel R D, Wilson B C, Li R K and Vitkin I A 2010 *J. Biomed. Opt.* **15** 047009
[38] Ghosh N, Wood M F and Vitkin I A 2010 *Opt. Commun.* **283** 1200–8
[39] Li P, Tariq A, He H and Ma H 2020 *Opt. Lett.* **45** 706–9
[40] Ossikovski R 2011 *Opt. Lett.* **36** 2330–2
[41] Ortega-Quijano N and Arce-Diego J L 2011 *Opt. Lett.* **36** 1942–4
[42] Ortega-Quijano N and Arce-Diego J L 2011 *Opt. Lett.* **36** 2429–31
[43] He H, Zeng N, Du E, Guo Y, Li D, Liao R and Ma H 2013 *Photonics Lasers Med.* **2** 129–37
[44] Khaliq A, Ashraf S, Gul B and Ahmad I 2021 *Opt. Commun.* **485** 126756
[45] Sheng W, Li W, Qi J, Liu T, He H, Dong Y, Liu S, Wu J, Elson D S and Ma H 2019 Quantitative analysis of 4 × 4 Mueller matrix transformation parameters for biomedical imaging *Photonics* **6** 34
[46] Sun M, He H, Zeng N, Du E, Guo Y, Liu S, Wu J, He Y and Ma H 2014 *Biomed. Opt. Express* **5** 4223–34
[47] Gil J J 2016 *J. Opt. Soc. Am.* A **33** 52–8
[48] Li P, Lv D, He H and Ma H 2018 *Opt. Express* **26** 3791–800
[49] Dong Y, Wan J, Si L, Meng Y, Dong Y, Liu S, He H and Ma H 2021 *IEEE Trans. Biomed. Eng.* **68** 881–92
[50] Arteaga O, Baldrís M, Antó J, Canillas A, Pascual E and Bertran E 2014 *Appl. Opt.* **53** 2236–45
[51] Zhou J, He H, Chen Z, Wang Y and Ma H 2018 *J. Biomed. Opt.* **23** 016007
[52] Chen Z, Meng R, Zhu Y and Ma H 2020 *Opt. Laser Eng.* **129** 106055
[53] Saytashev I, Saha S, Chue-Sang J, Lopez P, Laughrey M and Ramella-Roman J C 2020 *Opt. Lett.* **45** 2168–71
[54] Vizet J *et al* 2017 *Sci. Rep.* **7** 1–12
[55] Gonzalez M, Montejo K A, Krupp K, Srinivas V, DeHoog E, Madhivanan P and Ramella-Roman J C 2020 *J. Biomed. Opt.* **25** 116006
[56] Qi J, Ye M, Singh M, Clancy N T and Elson D S 2013 *Biomed. Opt. Express* **4** 2433–49
[57] Qi J and Elson D S 2016 *Sci. Rep.* **6** 1–11
[58] Vizet J, Manhas S, Tran J, Validire P, Benali A, Garcia-Caurel E, Pierangelo A, De Martino A and Pagnoux D 2016 *J. Biomed. Opt.* **21** 071106
[59] Rivet S, Bradu A and Podoleanu A 2015 *Opt. Express* **23** 23768–86
[60] Fu Y, Huang Z, He H, Ma H and Wu J 2018 *IEEE T. Instrum. Meas.* **67** 1700–12
[61] Wang J, Zheng W, Lin K and Huang Z 2016 *Biomed. Opt. Express* **7** 1116–26
[62] Golaraei A *et al* 2014 *Biomed. Opt. Express* **5** 3562–7
[63] Jiao S and Wang L V 2002 *Opt. Lett.* **27** 101–3
[64] Gil J J and Ossikovski R 2016 *Polarized Light and the Mueller Matrix Approach* (Boca Raton, FL: CRC Press)
[65] Manhas S, Swami M, Buddhiwant P, Ghosh N, Gupta P and Singh K 2006 *Opt. Express* **14** 190–202
[66] Guo Y, Zeng N, He H, Yun T, Du E, Liao R, He Y and Ma H 2013 *Opt. Express* **21** 18361–70
[67] Ossikovski R and Vizet J 2017 *Appl. Opt.* **56** 8446–51
[68] Qi J, He H, Ma H and Elson D S 2017 *Opt. Lett.* **42** 4048–51
[69] Ossikovski R, Anastasiadou M and De Martino A 2008 *Opt. Commun.* **281** 2406–10

[70] Ossikovski R and De Martino A 2015 *J. Opt. Soc. Am.* A **32** 343–8
[71] Li P, Lee H R, Chandel S, Lotz C, Groeber-Becker F K, Dembski S, Ossikovski R, Ma H and Novikova T 2020 *J. Biomed. Opt.* **25** 015002
[72] Lee H R *et al* 2019 *J. Biomed. Opt.* **24** 076004
[73] Cloude S R 1986 *Optik* **75** 26–36
[74] Cloude S R 1990 Conditions for the physical realisability of matrix operators In polarimetry *Proc. SPIE* **1166**
[75] Simon R 1982 *Opt. Commun.* **42** 293–7
[76] Barakat R 1996 *Opt. Commun.* **123** 443–8
[77] Brosseau C 1998 *Fundamentals of Polarized Light: A Statistical Optics Approach* (New York: Wiley-Interscience)
[78] Gil J J 2007 *Eur. Phys. J. Appl. Phys.* **40** 1–47
[79] San José I and Gil J J 2011 *Opt. Commun.* **284** 38–47
[80] Gil J J and Bernabeu E 1985 *Opt. Acta: Int. J. Opt.* **32** 259–61
[81] Tariq A, Li P, Chen D, Lv D and Ma H 2017 *Phys. Rev. Lett.* **119** 033202
[82] Aiello A and Woerdman J 2005 *Phys. Rev. Lett.* **94** 090406
[83] van de Hulst H C 1981 *Light Scattering by Small Particles* (New York: Dover)
[84] Pravdin A B, Yakovlev D A, Spivak A V and Tuchin V V 2005 *Proc. SPIE* **5695** 303–11
[85] Steeg G V and Galstyan A 2014 Discovering structure in high-dimensional data through correlation explanation *Adv. Neural Inf. Process. Syst.* **1** 577–85
[86] Si L, Li X, Zhu Y, Sheng Y and Ma H 2020 *Opt. Express* **28** 10456–66
[87] Jiang X, Zeng N and He Y 2007 *Prog. Biochem. Biophys.* **34** 659
[88] Arteaga O, Garcia-Caurel E and Ossikovski R 2011 *J. Opt. Soc. Am.* A **28** 548–53
[89] He H, Sun M, Zeng N, Du E, Liu S, Guo Y, Wu J, He Y and Ma H 2014 *J. Biomed. Opt.* **19** 106007